

# Catalytic oxidation of *n*-octane over cobalt substituted ceria ( $\text{Ce}_{0.90}\text{Co}_{0.10}\text{O}_{2-\delta}$ ) catalysts

Mahadevaiah Narayanappa, Venkata D.B.C. Dasireddy, Holger B. Friedrich\*

Catalysis Research Group, School of Chemistry, University of KwaZulu-Natal, Westville Campus, Durban 4000, South Africa

## ARTICLE INFO

### Article history:

Received 18 June 2012

Received in revised form 6 September 2012

Accepted 12 September 2012

Available online 22 October 2012

### Keywords:

Cobalt substituted ceria

Ce–Co ionic catalysts

*n*-Octane

1-Octene

Styrene

Oxidative dehydrogenation

## ABSTRACT

Catalytic oxidative activation of octane was carried out in the presence of Co substituted ceria catalysts of the type  $\text{Ce}_{1-x}\text{Co}_x\text{O}_{2-\delta}$  ( $\text{Ce}_{0.90}\text{Co}_{0.10}\text{O}_{2-\delta}$ ). The catalysts were synthesized by the solution combustion method and the surface characteristics were determined by BET, powder XRD, structural refinement and XPS. The synthesized catalyst crystallizes with a fluorite structure, the crystallinity was confirmed by bright-field images of TEM. Hydrogen uptake studies show a strong reduction peak at 425 °C and it proves substitution of cobalt ions inside the matrix of the lattice system. X-ray photoelectron spectroscopy (XPS) clarified that even though under reduction conditions, the cerium ions were slightly oxidized because of the sequence of standard reduction potentials of both cerium and cobalt ions. The catalytic activity of the catalyst was investigated between the temperature range from 350 to 550 °C, in a continuous flow fixed bed reactor at GHSV 4000 h<sup>-1</sup> with varying *n*-octane to oxygen molar ratios from 1:0.5 to 1:2.5. Results show that the conversion and selectivity of products (alkenes, oxygenates, aromatics, carbon oxides and cracked products) from the *n*-octane varies consequently with *n*-octane to oxygen molar ratio. The product selectivity at iso-conversion for C<sub>8</sub> products, aromatics, oxygenates and octenes was determined. The catalyst shows higher activity with respect to an increase in the *n*-octane to oxygen molar ratio and reaction temperature.

© 2012 Elsevier B.V. All rights reserved.

## 1. Introduction

Cerium oxide has been widely investigated due to its multiple applications; as a catalyst, an electrolyte material of solid oxide fuel cells, a material of high refractive index, etc. [1–3]. Due to the special and favorable properties of ceria such as redox, acid–base and oxygen storage capacity [4,5], it has considerable significance in the area of industrial catalysis for the oxidation of hydrocarbons [6–8] and these properties of ceria either alone or with transition metals are important parameters in facilitating several organic reactions [9].

Due to the high effectiveness of ceria oxide used as a support and the low cost of cobalt, these materials can form a highly active and selective catalytic system [10–16]. These materials are used in the field of CO oxidation [17], hydrogenation reactions [18], formation of hydrogen peroxide from oxygen and hydrogen [19], the water gas shift reaction [20] and automotive catalysis [21–23].

Ceria has the fluorite structure, with cerium ions at the corners and face center of the cube and the oxygen atoms in tetrahedral positions, but the activity of ceria-based catalyst depends greatly on its structure and nanosized ceria shows higher activity than

bulk-phase ceria, because of the easier reduction of the surface oxygen species on ceria nanoparticles [24]. Ceria can be employed as an oxide carrier or a mixed oxide carrier with a transition metal oxide providing unique catalytic properties [25,26]. A number of ceria-based systems such as,  $\text{CeO}_2/\text{Al}_2\text{O}_3$ ,  $\text{CuO}/\text{CeO}_2$ ,  $\text{CeO}_2/\text{SiO}_2$ ,  $\text{Pt}/\text{CeO}_2$ ,  $\text{Rh}/\text{CeO}_2$ ,  $\text{CeO}_2/\text{ZrO}_2$ ,  $\text{Pd}/\text{CeO}_2$  and  $\text{Au}/\text{CeO}_2$  have been studied for their catalytic properties [27–36].

Substitution of transition metals or noble metals in sites of cerium in the  $\text{CeO}_2$  matrix by solid–solid reaction to give  $\text{Ce}_{1-x}\text{M}_x\text{O}_{2-\delta}$  (M=Cu, Fe, Mn, Pt, Pd, Rh, Ru, Cr, Ni) has been reported [37]. Ceria influences the catalytic activity of the supported metal by the metal–support interaction. In addition to the metal support interaction the supported metal can also influence the physicochemical properties of the ceria support such as the oxygen storage capacity,  $\text{Ce}^{4+}/\text{Ce}^{3+}$  redox couple, and the defect sites such as anionic vacancies at the metal–ceria interface can directly contribute to the catalytic activity of the ceria-supported metals [31,38,39]. The enhancement in the catalytic activity of ceria supported materials is also due to the redox potential of  $\text{Ce}^{4+}/\text{Ce}^{3+}$  (1.61 V), which is higher than some of the reduction potentials of 3d transition metals like  $\text{Cr}^{6+}/\text{Cr}^{3+}$  (1.33 V),  $\text{Fe}^{3+}/\text{Fe}^{2+}$  (0.77 V),  $\text{Mn}^{3+}/\text{Mn}^{2+}$  (1.51 V) or  $\text{Cu}^{2+}/\text{Cu}^0$  (0.34 V) and it has been shown that substituted transition metal ions remain in the oxidized form in the  $\text{CeO}_2$  matrix [37]. In the cobalt substituted ceria matrix, the redox potential of  $\text{Co}^{3+}/\text{Co}^{2+}$  (1.81 V) is higher than the reduction

\* Corresponding author. Tel.: +27 31 2603107; fax: +27 31 2603091.  
E-mail address: [friedric@ukzn.ac.za](mailto:friedric@ukzn.ac.za) (H.B. Friedrich).

potential of  $\text{Ce}^{4+}/\text{Ce}^{3+}$  (1.6 V), therefore  $\text{Co}^{2+}$  should be more stable in the presence of  $\text{Ce}^{4+}$ . However, under strongly oxidizing conditions the redox potential of  $\text{Co}^{3+}/\text{Co}^{2+}$  (1.42 V) [40] is lower than that of  $\text{Ce}^{4+}/\text{Ce}^{3+}$ , therefore  $\text{Co}^{3+}$  is more stable and the Co ions in the 2+ as well the 3+ states are thus stable in  $\text{CeO}_2$ .

The extent of catalytic activity of transition metal ion substituted ceria also depends upon the preparative method of the composite oxide. For example a copper substituted cerium oxide prepared by the combustion method shows different low temperature reduction features compared to the same material prepared by other conventional methods [24].

Cobalt in ceria and its composites have been found to be selective redox catalysts for the production of lower alkenes and higher *n*-alkanes from syngas [41,42]. The presence of metal ions in the ceria lattice has been studied from the point of their redox and catalytic properties in several catalytic transformations such as steam reforming, oxidative adsorption of nitric oxide, oxidation of carbon monoxide and the total oxidation of hydrocarbons [40,43–45].

In the present work we have synthesized the cobalt substituted ceria of the type  $\text{Ce}_{1-x}\text{Co}_x\text{O}_{2-\delta}$  ( $0 \leq x \leq 0.20$ ) solid-solid sol by the solution combustion method, studied their structure and investigated their catalytic activity in the oxidation of octane.

## 2. Experimental

### 2.1. Preparation of the catalyst

$\text{Ce}_{1-x}\text{Co}_x\text{O}_{2-\delta}$  ( $x = 0.10, 0.15, 0.20$  and  $0.35 \leq \delta \leq 0.40$ ) was synthesized by the single step solution combustion method [8]. For the preparation of the  $\text{Ce}_{0.90}\text{Co}_{0.10}\text{O}_{2-\delta}$  catalyst, 4.93 g of  $(\text{NH}_4)_2\text{Ce}(\text{NO}_3)_6$  (Sigma–Aldrich, 99.9%), 0.29 g  $\text{Co}(\text{NO}_3)_2 \cdot 5\text{H}_2\text{O}$  (Sigma–Aldrich, 99.9%) and 3.46 g of  $\text{NH}_2\text{CONH}_2$  were dissolved in a minimum volume of water ( $\sim 50 \text{ cm}^3$ ) in a borosilicate dish. The solution was heated on a hot plate till the solution boils, then the solution containing glass dish was kept in a muffle furnace at  $\sim 400^\circ\text{C}$ . The solution boils with frothing, followed by complete dehydration and burns with a flame yielding a voluminous solid product. The same procedure was followed to prepare  $\text{Ce}_{0.85}\text{Co}_{0.15}\text{O}_{2-\delta}$  and  $\text{Ce}_{0.80}\text{Co}_{0.20}\text{O}_{2-\delta}$  catalysts by adding stoichiometric calculated amounts of  $(\text{NH}_4)_2\text{Ce}(\text{NO}_3)_6$ ,  $\text{Co}(\text{NO}_3)_2 \cdot 5\text{H}_2\text{O}$  and  $\text{NH}_2\text{CONH}_2$ .

### 2.2. Catalyst characterization

The BET surface area and pore volume of the catalyst was analyzed after the degassing (at  $150^\circ\text{C}$ ) of the sample using a Micromeritics ASAP 2020 multi-point BET surface area analyzer. X-ray diffraction patterns were recorded with Philips X'Pert diffractometer at the scanning rate  $0.5^\circ/\text{s}$  between the  $2\theta$  ranges from  $10^\circ$  to  $90^\circ$ . The structural refinements were carried out using Full Prof Suite-2000 version [46]. Hydrogen uptake experiments for the catalyst were carried out in a continuous flow quartz micro-reactor of length 30 cm and 0.5 cm internal diameter with 5.15%  $\text{H}_2/\text{Ar}$  mixture flowing at 17 mL/min with a linear heating rate of  $5^\circ\text{C}/\text{min}$ . A thermal conductivity detector (TCD) was used to monitor the amount of hydrogen consumed during the experiments. After the first cycle, the catalyst was oxidized by passing oxygen at  $500^\circ\text{C}$  for 30 min, then the catalyst was cooled to the room temperature and a second run was carried out. Ammonia temperature programmed desorption (TPD) was carried out using a Micromeritics 2920 Autochem II Chemisorption Analyser. In the TPD experiments, the temperature was set to  $950^\circ\text{C}$  with a ramping rate of  $10^\circ\text{C}/\text{min}$  using helium as the carrier gas. X-ray photo electron spectra (XPS) were recorded with Thermo Scientific Multilab 2000 equipment by employing Al-K $\alpha$  radiation (1486.6 eV) and

considering the C (1s) spectra as the reference (284.5 eV) for all binding energies. Transmission electron microscopy (TEM) images were viewed on a Jeol JEM-1010 electron microscope. The images were captured and analyzed by using iTEM software. High resolution TEM images were recorded by using Jeol JEM 2100 Electron Microscope.

### 2.3. Catalytic studies

Gas phase oxidation of octane was carried out in a continuous gas flow fixed bed reactor between the temperature range from  $350$  to  $550^\circ\text{C}$ . A tubular stainless steel reactor tube with a 10 mm internal diameter and 300 mm length was used to load the catalyst. The catalyst was pelletized and sieved through the mesh size 600–1000  $\mu\text{m}$ . 1 ml of the catalyst was placed at the center of the reactor tube and plugged the both ends with carborundum crystals (size 24-grit). K-type thermocouples were used to monitor the change in temperature at the catalytic bed and in the reactor furnace and the thermocouples were controlled by CB-100 RK temperature control units. The *n*-octane feed was delivered into the reactor system using a high precision isocratic pump (Lab Alliance Series II). The catalytic tests were carried out at different *n*-octane to oxygen molar ratios and the GHSV of  $4000 \text{ h}^{-1}$ . The concentration of *n*-octane in the gaseous mixture was maintained as 11.3% (v/v). Air was used as an oxidant and nitrogen used as diluent to make-up and achieve the total gas flow rate 90 mL/min. The total volume of the gaseous products at the outlet were measured using a wet gas flow meter (Ritter Drum-Type Gas Meter). The main catalyzed products (gaseous and liquid) were analyzed by using Perkin Elmer Clarus 400 FID and TCD gas chromatographs. In the GC, the flame ionization detector (FID) connected to a SGE BP-PONA capillary column (0.25 mm ID and 50 m length) was used to analyze the organic products at oven temperatures ramping between 40 and  $200^\circ\text{C}$ . The thermal conductivity detector (TCD) with a SUPELCO Carboxen (0.53 mm ID and 30 m length) column was used to analyze the carbon oxides. A Perkin Elmer Clarus 500 GC-MS was used to identify unknown products from the reaction stream. The calculated carbon balance was between 97 and 100%. All data points were obtained in duplicate with an error of  $\pm 2\%$ .

## 3. Results and discussion

### 3.1. Powder catalyst textural and morphological characterization

#### 3.1.1. Powder catalyst X-ray diffractogram and Rietveld refinement studies

The powder XRD patterns of different substitutions (10, 15 and 20 atomic%) of cobalt in ceria are shown (Fig. 1). The XRD profiles show that pure (complete) substitution takes place only for the 10% cobalt substituted  $\text{Ce}_{0.90}\text{Co}_{0.10}\text{O}_{2-\delta}$  catalyst (Fig. 1(a)) but for the other  $\text{Ce}_{0.85}\text{Co}_{0.15}\text{O}_{2-\delta}$  and  $\text{Ce}_{0.80}\text{Co}_{0.20}\text{O}_{2-\delta}$  (15 and 20% of cobalt substituted) catalysts an additional peak occurred due to the formation of cobalt oxides (Fig. 1b and c). Thus, for further studies, only the 10% cobalt substituted ceria ( $\text{Ce}_{0.90}\text{Co}_{0.10}\text{O}_{2-\delta}$ ) catalyst was considered.

The XRD profiles were refined with varying background parameters such as scale factor, unit cell, shape, and isotropic thermal parameters. The Rietveld refined XRD profiles of the 10% cobalt substituted catalyst ( $\text{Ce}_{0.90}\text{Co}_{0.10}\text{O}_{2-\delta}$ ) are shown (Fig. 1(e)) and the refined XRD data and other surface properties of the catalysts are summarized in Table 1. A slight increase in the lattice parameters in the cobalt substituted ceria is observed. This increase in the lattice parameter is due to the partial reduction of Ce from the 4+ to 3+ state and it is confirmed by XPS studies.

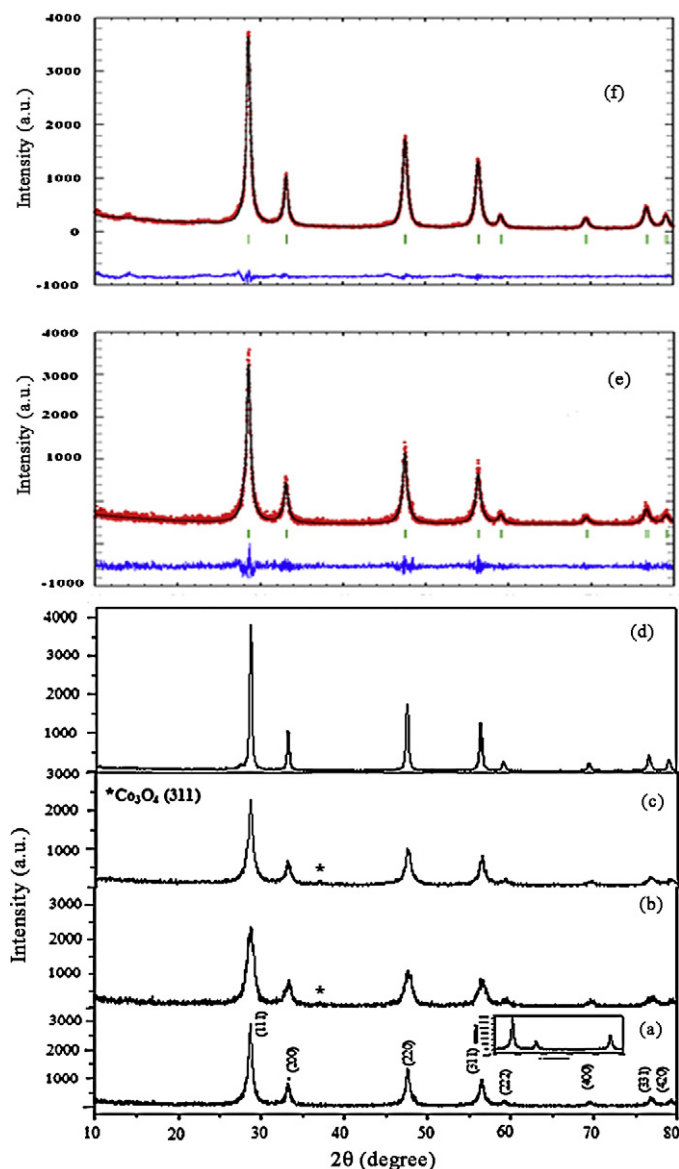


**Fig. 1.** Powder XRD patterns of (a)  $\text{Ce}_{0.90}\text{Co}_{0.10}\text{O}_{2-\delta}$  catalyst (inset: slow scan rate between  $25^\circ$  and  $50^\circ$  of  $\text{Ce}_{0.90}\text{Co}_{0.10}\text{O}_{2-\delta}$  catalyst), (b)  $\text{Ce}_{0.85}\text{Co}_{0.15}\text{O}_{2-\delta}$ , (c)  $\text{Ce}_{0.80}\text{Co}_{0.20}\text{O}_{2-\delta}$ , (d) spent  $\text{Ce}_{0.90}\text{Co}_{0.10}\text{O}_{2-\delta}$  catalyst and Rietveld refined XRD profiles of  $\text{Ce}_{0.90}\text{Co}_{0.10}\text{O}_{2-\delta}$  catalyst, (e) freshly prepared and (f) after  $\text{H}_2$  reduction at  $500^\circ\text{C}$ .

### 3.1.2. BET surface area and pore volume measurements

The measured surface area and pore volume of the freshly prepared  $\text{Ce}_{0.90}\text{Co}_{0.10}\text{O}_{2-\delta}$  catalyst are  $63.7\text{ m}^2\text{g}^{-1}$  and  $0.09\text{ cm}^3\text{g}^{-1}$  respectively. Nitrogen adsorption–desorption experiments revealed that the catalyst was porous and the adsorption isotherms of the type IV confirm that the samples is mesoporous in nature [47]. Pore-size distribution curves calculated from the desorption branch of the isotherms indicate the presence of mesoporosity in

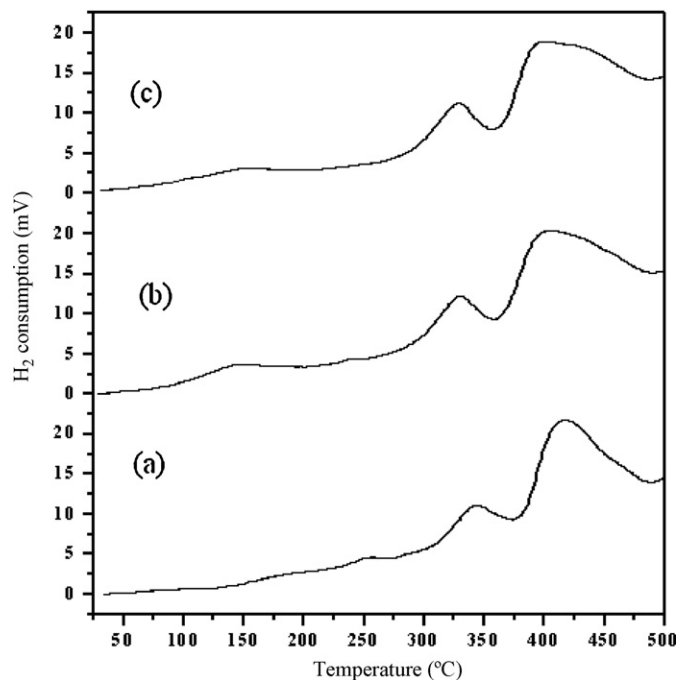


**Fig. 2.** Temperature programmed reduction (TPR) profiles of  $\text{Ce}_{0.90}\text{Co}_{0.10}\text{O}_{2-\delta}$  catalysts (a) 1st cycle, (b) 2nd cycle and (c) 3rd cycle reduced by  $\text{H}_2$  at  $500^\circ\text{C}$ .

the catalyst (the adsorption isotherms and poresize distribution curves are given in the [additional results](#)).

### 3.1.3. Powder catalyst redox studies

**Fig. 2** shows the TPR profiles for the  $\text{Ce}_{0.90}\text{Co}_{0.10}\text{O}_{2-\delta}$  catalyst in consecutive cycles. After every cycle, oxygen was passed through the catalyst for 30 min at  $500^\circ\text{C}$ , and the catalyst cooled to room temperature, then the TPR experiments were repeated. As can be seen from **Fig. 2**, the TPR profile repeats and reduction occurs in multiple steps. The major hydrogen uptake peaks are observed at the temperatures of  $325^\circ\text{C}$  and  $400^\circ\text{C}$ . The amount of total hydrogen consumption was calculated up to the temperature of  $500^\circ\text{C}$  as  $563\text{ }\mu\text{mol/g}$ ,  $545\text{ }\mu\text{mol/g}$  and  $551\text{ }\mu\text{mol/g}$  for the first, second and third cycles, respectively. The TPR curves show two peaks of reduction. The first peak is assigned to the reduction of  $\text{Co}^{3+}$  to  $\text{Co}^{2+}$  and the other to the reduction of  $\text{Co}^{2+}$  to  $\text{Co}^0$ . The Rietveld refined XRD profile of  $\text{Ce}_{0.90}\text{Co}_{0.10}\text{O}_{2-\delta}$  after the third TPR cycle is shown in **Fig. 1(f)** and it clearly confirms that  $\text{Ce}_{0.90}\text{Co}_{0.10}\text{O}_{2-\delta}$  retains its fluorite structure even after successive TPR cycles.

### 3.1.4. HR-TEM studies

The bright-field and HRTEM images of  $\text{Ce}_{0.90}\text{Co}_{0.10}\text{O}_{2-\delta}$  are shown in **Fig. 3a** and **b**. The inset of **Fig. 3a** shows the electron diffraction pattern and the ring pattern can be indexed to a fluorite structure. Lattice fringes with HRTEM are  $3.1\text{ \AA}$ , corresponding to the  $d(111)$  of the  $\text{Ce}_{0.90}\text{Co}_{0.10}\text{O}_{2-\delta}$  catalyst which indicates a high crystallinity of Co substituted  $\text{CeO}_2$ . The crystallite sizes in the catalyst are in the range of  $14 \pm 2\text{ nm}$ , these sizes are in good agreement with the values obtained from the XRD data. Thus the data from XRD

**Table 1**  
Surface properties and Rietveld refined data of cobalt substituted ceria catalyst.

Catalysts	Surface area ( $\text{m}^2/\text{g}$ )	Pore volume ( $\text{cm}^3/\text{g}$ )	Lattice parameters ( $\text{\AA}$ )	Structure factor ( $R_f$ )	Bragg factor ( $R_B$ )
$\text{Ce}_{0.90}\text{Co}_{0.10}\text{O}_{2-\delta}$ As prepared	63.7	0.09	5.417(6)	1.9	3.2
$\text{Ce}_{0.90}\text{Co}_{0.10}\text{O}_{2-\delta}$ Spent catalyst	63.3	0.09	5.413(9)	1.7	3.2
$\text{CeO}_2$ As prepared (heated at $500^\circ\text{C}$ )	67.8	0.07	5.409(3)	1.2	2.2

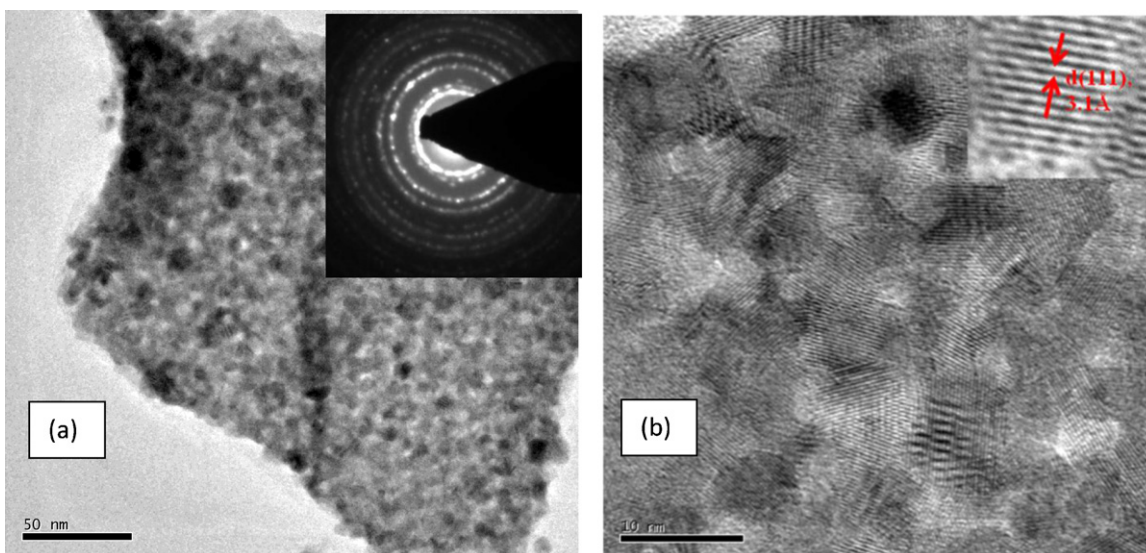


Fig. 3. (a) Bright-field image and electron diffraction pattern and (b) HRTEM images of  $\text{Ce}_{0.90}\text{Co}_{0.10}\text{O}_{2-\delta}$  catalyst.

and TEM studies confirm the formation of a solid–solid solution of  $\text{Ce}_{0.90}\text{Co}_{0.10}\text{O}_{2-\delta}$ .

### 3.1.5. X-ray photon spectroscopy (XPS) studies

The oxidation states of Co and Ce in freshly-prepared  $\text{Ce}_{0.90}\text{Co}_{0.10}\text{O}_{2-\delta}$  were determined by XPS and the core level XPS of Co (2p) of  $\text{Ce}_{0.90}\text{Co}_{0.10}\text{O}_{2-\delta}$  is shown in Fig. 4. In general, Co is in the +2 oxidation state and occurs with high spin. The  $\text{Co}^{2+}$ (2p) region is characterized by a large satellite peak at  $\sim 5.5$  eV below the main peak [48]. But in freshly prepared  $\text{Ce}_{0.90}\text{Co}_{0.10}\text{O}_{2-\delta}$ , a satellite peak below the main peak (780.3 eV) was not found (Fig. 4(a)). Therefore, Co is not (only) in the +2 state but may likely be in both the +2 and +3 state (mixed valence) [49], it is possible even that Co may get oxidized to the +4 state under higher oxidizing conditions of the preparation.

Upon reduction with hydrogen,  $\text{Co}^{3+}$  gets reduced to the  $\text{Co}^{2+}$  state and that can be seen from the  $\text{Co}(2p_{3/2})$  peak at 780.3 eV with a strong satellite peak (Fig. 4(b)). But the spent catalyst shows the  $\text{Co}^{2+}$  ion may get partially oxidized to  $\text{Co}^{3+}$  (Fig. 4(c)). As seen from the XPS study  $\text{Co}(2p_{3/2})$  binding energies, the cobaltous ( $\text{Co}^{2+}$ ) compounds normally vary between 780 and 782 eV, while those in cobaltic ( $\text{Co}^{3+}$ ) compounds are typically in the range 779–782 eV. Hence it is difficult to identify the oxidation states of cobalt on the basis of the chemical shift of the binding energy [49] (Core level XPS of Ce(3d) in  $\text{Ce}_{0.90}\text{Co}_{0.10}\text{O}_{2-\delta}$  is shown in Fig. 4(d)). The  $\text{Ce}^{4+}(3d_{5/2})$  peak obtained at 882.5 eV is a characteristic of  $\text{Ce}^{4+}$  in  $\text{CeO}_2$  [50]. The  $\text{Ce}^{3+}(3d)$  in  $\text{Ce}_2\text{O}_3$  is characterized by  $\text{Ce}^{3+}(3d_{5/2})$  at 883.3 eV. Thus, partial filling of the valley between  $\text{Ce}^{4+}(3d_{5/2})$  at  $\sim 881$  eV and its satellite at 886.5 eV shows that Ce is in a mixed valence state (+4, +3) [8,29]. The ratios of the oxidation states present in the catalyst ( $\text{Ce}^{4+}$  and  $\text{Ce}^{3+}$ ) were calculated as 0.84: 0.16. Upon the continuous reduction of the cobalt,  $\text{Ce}^{3+}$  gets oxidized to  $\text{Ce}^{4+}$  (Fig. 4(e)) and on re-oxidation; Ce continues to be present in the +4 state (Fig. 4(f)).

## 3.2. Catalytic activity studies

Catalytic experiments were performed in the temperature range between 350 and 550 °C using a fixed bed continuous gas flow reactor at a gas hourly space velocity (GHSV) of 4000  $\text{h}^{-1}$ . The conversion of octane to desirable products was achieved with the  $\text{Ce}_{0.90}\text{Co}_{0.10}\text{O}_{2-\delta}$  catalyst in the presence of oxygen from air. The major products observed during the oxidation of *n*-octane were octenes (1-octene, trans and cis 2-octene, trans 3-octene, trans

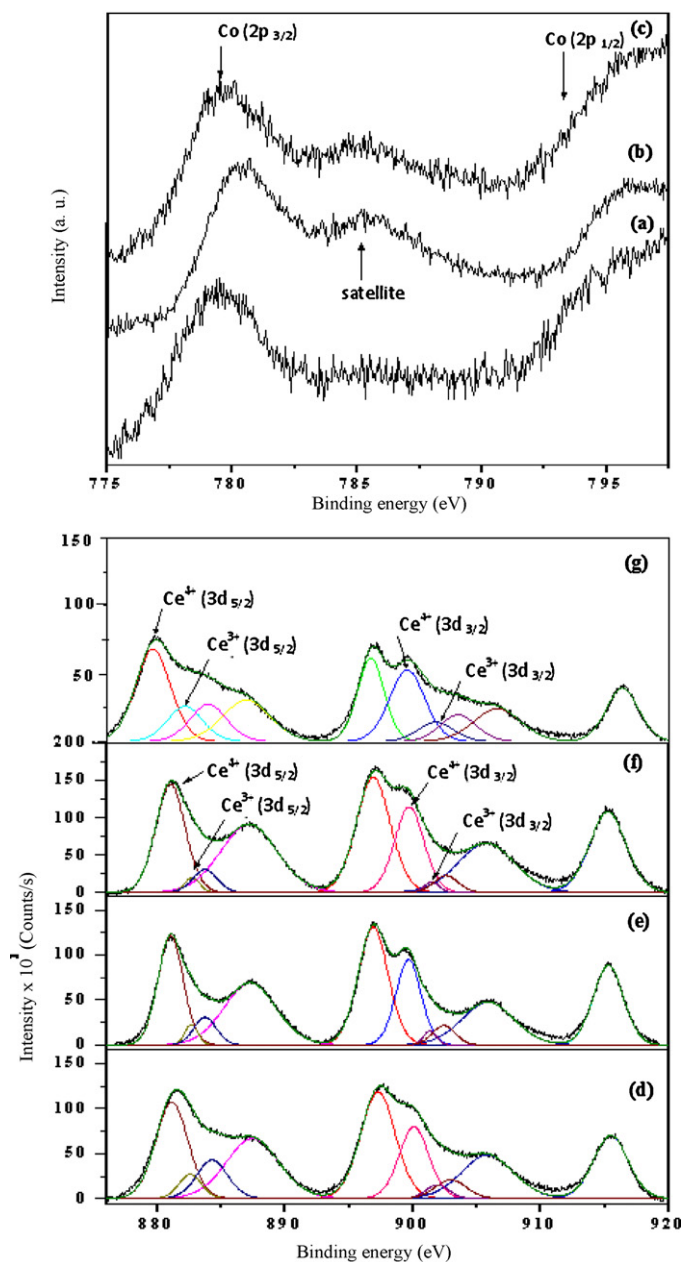
4-octene), oxygenates (octanal, 1-octanol, 2-octanol, 2-octanone, 3-octanone), carbon oxides (CO and  $\text{CO}_2$ ), aromatics (o-xylene, styrene, ethylbenzene) and a lower amount of cracked products. In addition the catalytic experiments were performed over  $\text{CeO}_2$  in order to compare the octane conversion (presence and absence of fed oxygen) with the cobalt substituted ceria catalyst, but no significant conversion was observed in the absence of cobalt ions in the ceria matrix (Fig. 5). The direct utilization of lattice oxygen of the  $\text{Ce}_{0.90}\text{Co}_{0.10}\text{O}_{2-\delta}$  catalyst was also studied for octane conversion in the absence of fed oxygen (Fig. 5) and only very low selectivity to oxygenates was observed. The conversion of octane in the absence of fed oxygen suggests that lattice oxygen is activated by the Co ion substitution in ceria and that fed  $\text{O}_2$  can be reversibly exchanged with lattice oxygen for the oxidation reaction.

Fig. 6(a) shows the effect of temperature and *n*-octane to oxygen feed ratio (*n*-octane:oxygen ( $\text{O}_2$ ), from 1:0.5 to 1:2.5) on octane conversion over  $\text{Ce}_{0.90}\text{Co}_{0.10}\text{O}_{2-\delta}$ . At a lower temperature, low conversion occurred due to the oxidation of octane by the surface reduction of cobalt. As the reaction progresses, octane gets oxidized by the bulk reduction of  $\text{Co}^{3+}$  at higher temperature. The reduced cobalt ( $\text{Co}^{2+}$ ) ions form the main defect centers and the created charge imbalance is neutralized by the formation of oxygen ion ( $\text{O}^{2-}$ ) vacancies ( $\text{O}^{2-}$  ions occupy the vacancies) for further oxidation [4,5].

Fig. 6(b) shows the conversion of oxygen with increase in temperature at different oxygen feed ratios. The assessment of the oxygen conversion reveals that the system is operating under aerobic conditions and supports the assumption that the reaction is predominantly oxidative. These results show that the oxygen conversion is proportional to the conversion of *n*-octane, because the redox properties of the catalyst play a crucial role in the reversible oxygen storage capacity (OSC) of  $\text{Ce}_{1-x}\text{Co}_x\text{O}_{2-\delta}$ , where oxidation of  $\text{Co}^{2+}$  to  $\text{Co}^{3+}$  occurred via  $\text{Ce}^{4+}$  to  $\text{Ce}^{3+}$  reduction when fed oxygen is exchanged with lattice oxygen.

### 3.2.1. Products formation and selectivity under different *n*-octane to oxygen molar feed ratios

Octenes are the major products at lower oxygen feed ratios (up to 1:1.5) (Fig. 7(a)). This is likely because a limited supply of oxygen favors the dehydrogenation of octane via reducing the  $\text{Co}^{3+}$  to  $\text{Co}^{2+}$  in the  $\text{Ce}_{0.90}\text{Co}_{0.10}\text{O}_{2-\delta}$  catalyst. But the selectivity toward the octenes decreases at higher temperature and higher oxygen feed ratios. The lower selectivity of octenes at higher feed oxygen



**Fig. 4.** Core level XPS of  $Ce_{(2p)}$  in  $Ce_{0.90}Co_{0.10}O_{2-\delta}$  (a) freshly prepared, (b) after  $H_2$  reduced at  $500^\circ C$ , (c) reoxidized by  $O_2$ , (d) spent catalyst and core level XPS of  $Co_{(2p)}$  in  $Ce_{0.90}Co_{0.10}O_{2-\delta}$ , (e) freshly prepared, (f) after  $H_2$  reduced at  $500^\circ C$  and (g) spent catalyst.

and higher temperature is countered by an increase in products such as oxygenates, aromatics, carbon oxides and cracked products [51,52]. Since an increase in selectivity toward carbon oxides at higher oxygen feed ratios is observed, coupled with a decrease in octene selectivity, these products may form by the secondary combustion of the octenes.

Fig. 7(b)) shows that the carbon oxides (CO and  $CO_2$ ) are formed at all temperatures. In the initial stages the amount of CO produced is almost the same as that of  $CO_2$ . These ratios are very nearly constant regardless of the initial feed to oxygen ratio up to 1:1.5. However, when the oxygen to feed ratio is high, the amount of  $CO_2$  formed increased. This is because, under strong oxidizing conditions, the cobalt is oxidized from  $Co^{2+}$  to  $Co^{3+}$  by creating an oxide ion vacancy in the metal lattice. These freely available oxide ions in

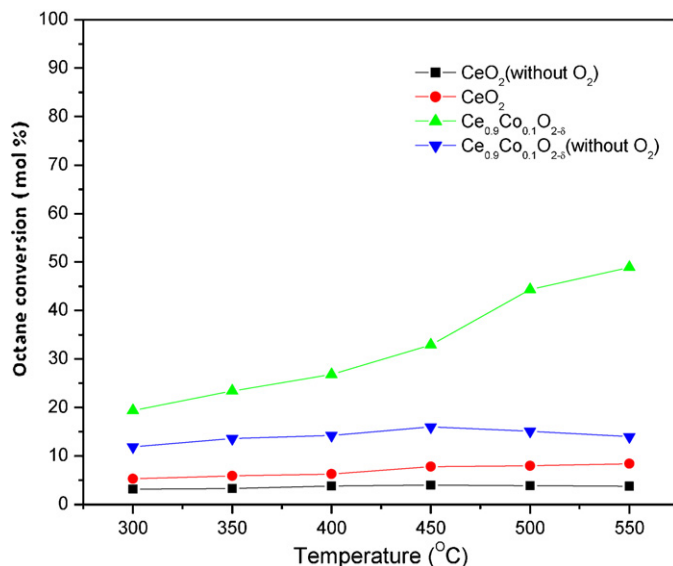


**Fig. 5.** Variation of Octane conversion with reaction temperature on  $CeO_2$  and  $Ce_{0.90}Co_{0.10}O_{2-\delta}$  (with and without feed  $O_2$ ) at  $GHSV\ 4000\ h^{-1}$ .

the lattice and oxygen species on the metal surface were capable forming  $CO_2$  through the secondary oxidation of CO.

Fig. 7(c) shows the selectivity toward the formation of oxygenates over  $Ce_{0.90}Co_{0.10}O_{2-\delta}$  catalyst at varying oxygen feed ratios. The selectivity of oxygenates increased up to a 1:2.0 feed to oxygen

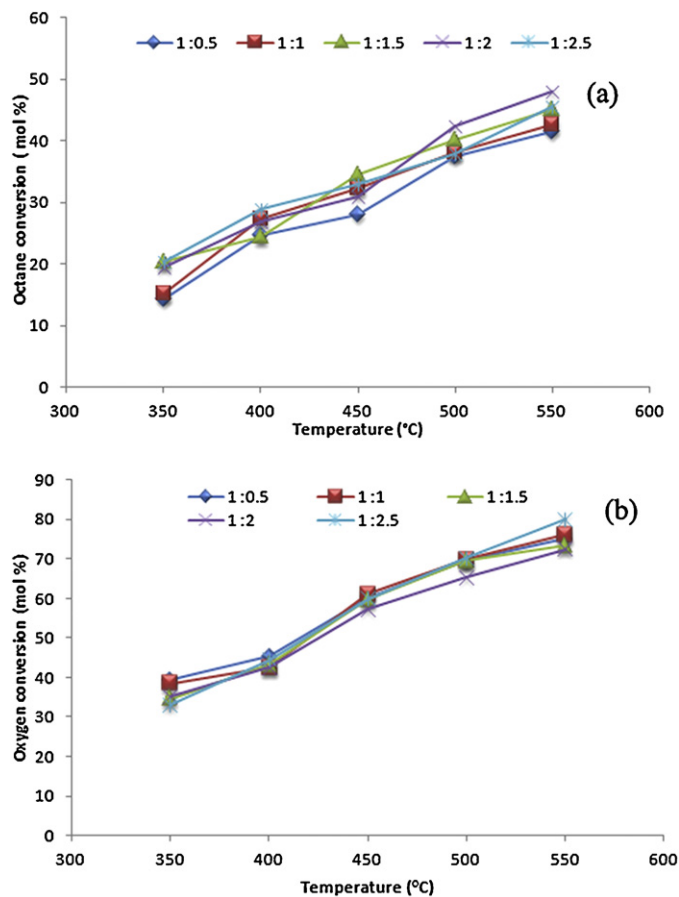


**Fig. 6.** Variation of (a) *n*-octane conversion and (b) oxygen conversion with reaction temperature and *n*-octane: oxygen feed ratios (from 1:0.5 to 1:2.5) at  $GHSV\ 4000\ h^{-1}$ .

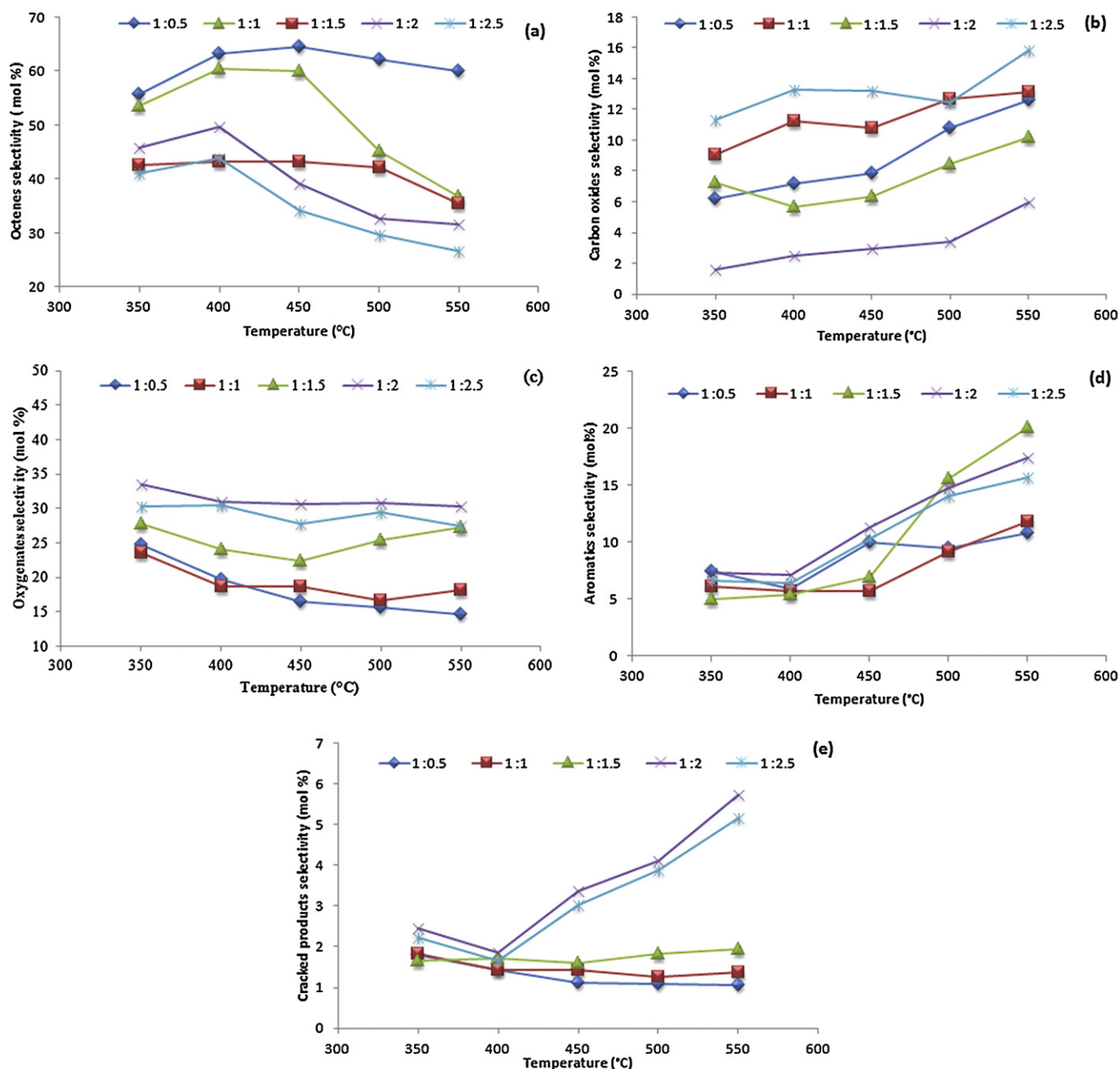


Fig. 7. Variation of products selectivity with reaction temperature and *n*-octane: oxygen feed ratios (from 1:0.5 to 1:2.5) at GHSV 4000 h<sup>-1</sup> over cobalt substituted ceria catalyst (a) octenes, (b) carbon oxides, (c) oxygenates, (d) aromatics and (e) cracked products.

ratio and decreased at the 1:2.5 feed to oxygen ratio. The increase in selectivity is because of the strong oxidizing environment around the redox cycle of the catalyst (Co<sup>3+</sup>/Co<sup>2+</sup> and Ce<sup>3+</sup>/Ce<sup>4+</sup>) which would be influencing the transfer of oxide ions through the lattice and it favors the dehydrogenation of octane and oxygen insertion into the octene to form the C<sub>8</sub> oxygenates. Also under oxidative conditions the production of oxygenates is influenced by the acidic nature of the catalyst [53].

The formation of aromatics was higher at higher oxygen feed ratios (Fig. 7(d)) which further favor the formation of the aromatics at higher temperatures (500–550 °C) [54,55]. This temperature is more consistent with the redox mechanism of the catalyst in which the oxide ion abstracts hydrogen from the octane. At the lower temperatures (300–350 °C) the selectivity of aromatics is lower compared with the other oxidative products in varying oxygen feed

ratios, because the dehydrogenation of octane was predominately an oxidative process through hydrogen abstraction by surface oxide ions. At the same time as the production of C<sub>8</sub> oxygenates, oxygen is continuing to insert to give cracked products. The selectivity of cracked products is higher at higher oxygen feed levels and higher temperature (Fig. 7(e)). The formation of cracked products can occur via steam and dry homogenous cracking and cracking is increased by the formation of water and carbon oxides [54,55].

### 3.2.2. Products distribution at iso-conversion of octane

The amount of products formed at a 32% isoconversion for the octane to oxygen ratios (1:0.5 to 1:2.5) is shown (Fig. 8). The product distribution obtained from *n*-octane conversion was octenes, oxygenates, aromatics, carbon oxides and cracked hydrocarbons. At the iso-conversion and lower

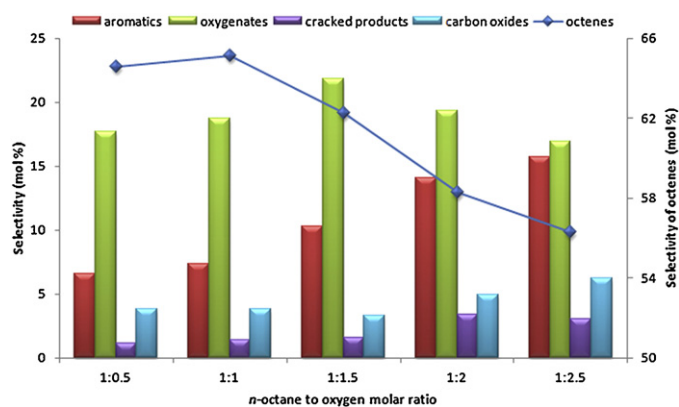


**Fig. 8.** Variation of the products distribution with *n*-octane:oxygen feed ratios (from 1:0.5 to 1:2.5) at iso-conversion of *n*-octane (at 450 °C) and GHSV 4000 h<sup>-1</sup>.

oxygen feed ratio octenes were dominantly formed and the order of production of octene isomers was 1-octene > trans-2-octene > trans-3-octene > cis-2-octene > trans-4-octene. Fig. 9(a) shows the production of isomers of octenes with increase in oxygen feed ratio. The selectivity of trans-2-octene is higher compared to cis-2-octene, due to the greater thermodynamic stability of the trans isomer. On the other hand no significant changes in the selectivity of 3-octenes with respect to the change in molar ratios were observed. Finally 4-octenes were found to be the least produced isomers in all cases. The low selectivity toward the formation of 4-octenes is because the elimination of hydrogen from the C<sub>4</sub> position is unfavorable in the activation of *n*-octane [53,55]. It is also affected by the homolytic capture of the C–H bond to form the surface alkyl

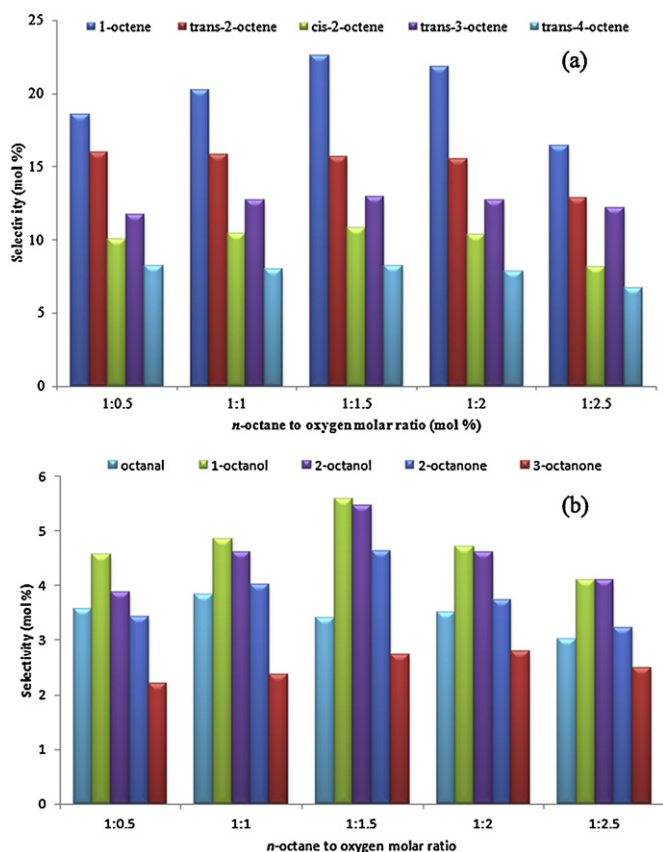


**Fig. 9.** Variation of the selectivity to (a) octenes and (b) oxygenates with *n*-octane:oxygen feed ratios (from 1:0.5 to 1:2.5) at iso conversion of *n*-octane and GHSV 4000 h<sup>-1</sup>.

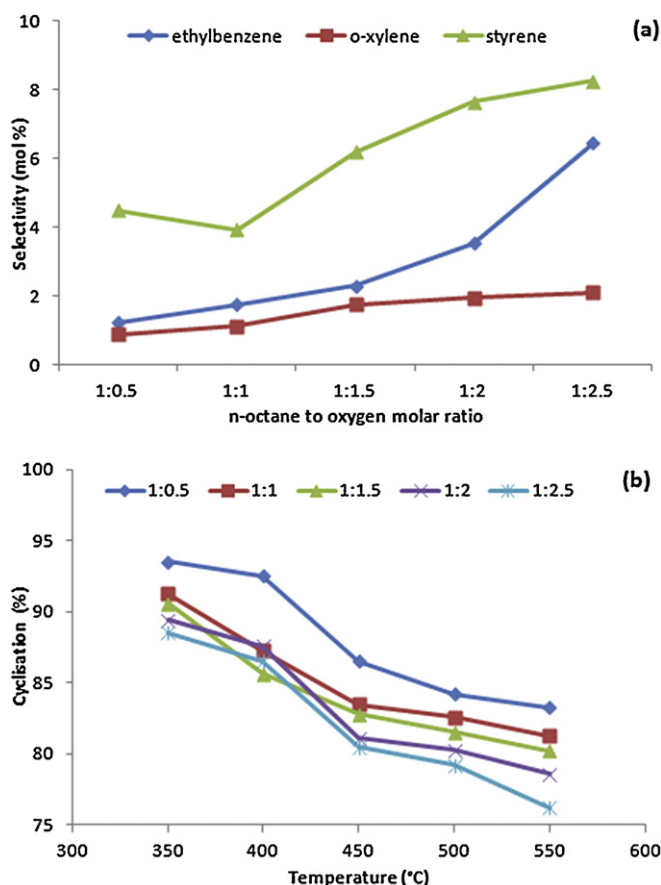


**Fig. 10.** Variation of the selectivity to (a) aromatics with *n*-octane:oxygen feed ratios (from 1:0.5 to 1:2.5) and (b) % 1,6 cyclisation with reaction temperature at iso-conversion of *n*-octane at GHSV 4000 h<sup>-1</sup>.

species, followed by the elimination of the second hydrogen from the neighboring carbon to form the olefin bond. Besides these thermodynamic factors, steric effects and the number of active centers are also responsible for the selectivity of octene isomers. By considering the mechanism of the alkane activation and by inspecting the relative abundances of octene isomers, it is possible to assume that *n*-octane activation has occurred more predominantly at C<sub>2</sub> and C<sub>1</sub> as compared to C<sub>4</sub>.

The selectivity toward the oxygenates at iso-conversion is shown in Fig. 9(b). 1-Octanol and 2-octanol are the major isomer products of the oxygenates, with a small amount of 3-octanone also forming. Product distribution of the major isomers of the oxygenates indicates that the carbon positions at C<sub>1</sub> and C<sub>2</sub> are more favorable to form 1-octanol and 2-octanol. The selectivity toward the oxygenates decreases with increase in oxygen feed ratio due to the influence of secondary combustion of oxygenates to form the carbon oxides.

The selectivity to C<sub>8</sub> aromatics exhibited a maximum at about 32% conversion. The product distribution of *n*-octane shows styrene as the dominant aromatic compound with small quantities of ethyl benzene and *o*-xylene (Fig. 10(a)) which are expected products from the direct closure to form the six-membered ring. Styrene is forming from the cyclisation of octane by bonding via C<sub>1</sub> to C<sub>6</sub>. In general, the cyclisation between the C<sub>1</sub> to C<sub>6</sub> and C<sub>2</sub> to C<sub>7</sub> leads to the formation of styrene/ethyl benzene and *o*-xylene respectively [56]. But here, the cyclisation that takes place through the C<sub>1</sub> to C<sub>6</sub> mode is more than 85% of the cyclic products (Fig. 10(b)). It is also observed that the percent of C<sub>1</sub> to C<sub>6</sub> cyclisation decreases with increase in feed to oxygen ratio. So it can be concluded from the above factors that C<sub>1</sub> to C<sub>6</sub> cyclisation is more favorable to form the

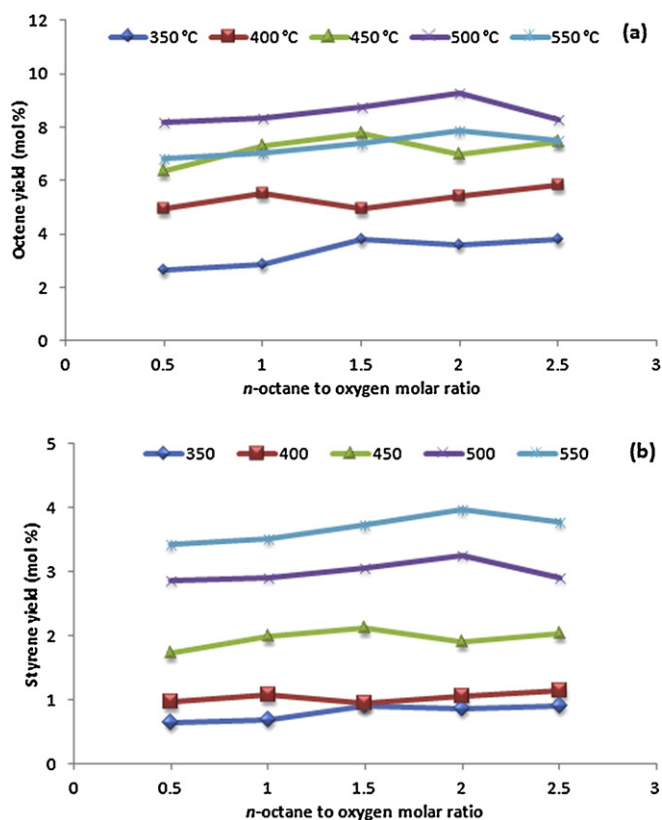


Fig. 11. Variation in the yield of products at varied temperatures with *n*-octane to oxygen feed ratios (from 1:0.5 to 1:2.5) at GHSV 4000 h<sup>-1</sup> (a) 1-octene and (b) styrene.

aromatics in the activation of *n*-octane. But the C<sub>2</sub> to C<sub>7</sub> cyclisation mode increases with increase in temperature and oxygen content.

The major aromatic products of *n*-octane are from the dehydrocyclization reaction by direct 1,6 ring closure. The dehydrogenation steps occur during the bifunctional mechanism, when *n*-octane is adsorbed on metal sites and the dehydrogenated species migrate to the acidic sites where they are hydroisomerized or hydro cracked. The dehydrogenated hydroisomerized products then migrate to metal sites for hydrogenation prior to desorption as 1-octene [57]. The yield of 1-octene was high at higher temperatures (Fig. 11(a)) and it confirms that 1-octene is preferentially consumed during the formation of aromatics at higher temperature and it allows 1,6 ring closure to lead to the cyclisation to form ethyl benzene and styrene [50,58].

The maximum yield of styrene was observed at higher temperature 500–550 °C (Fig. 11(b)) probably because higher temperature provides more energy to overcome the activation barrier to form the styrene. The slight decrease in the yield of styrene with increase in the oxygen feed might be due to the formation of carbon oxides from the secondary combustion of styrene.

The spent catalyst Ce<sub>0.90</sub>Co<sub>0.10</sub>O<sub>2-δ</sub> after four repeated cycles (between the temperatures 350 and 550 °C) of the oxidation of octane reactions was examined by XRD and XPS. No differences were observed in the catalyst structure compared to the freshly prepared catalyst. All the peaks were indexed to the fluorite structure and peaks corresponding to Co<sub>3</sub>O<sub>4</sub> were not observed in the XRD pattern (Fig. 1(d)). The oxidation state of the metal ion with the spent Ce<sub>0.90</sub>Co<sub>0.10</sub>O<sub>2-δ</sub> catalyst was determined by XPS. The core level Co(2p) spectrum of the spent Ce<sub>0.90</sub>Co<sub>0.10</sub>O<sub>2-δ</sub> catalyst is shown in Fig. 6(c) and suggested that the Co is mostly present in both the 2+ and the 3+ oxidation states. The core level Ce(3d) spectra of the spent Ce<sub>0.90</sub>Co<sub>0.10</sub>O<sub>2-δ</sub> catalyst is shown in Fig. 4(g). Ce

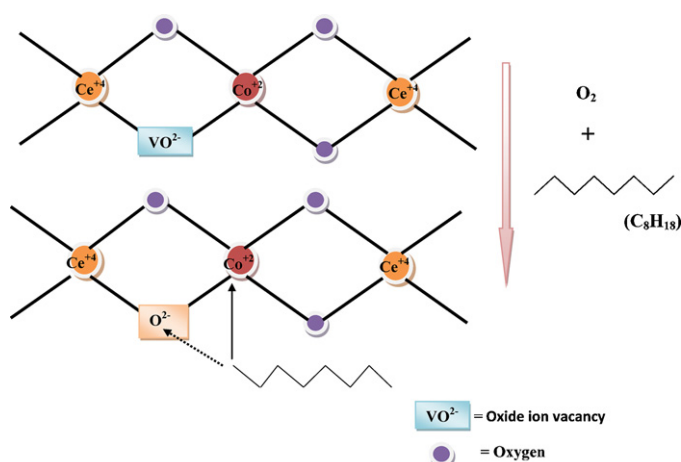


Fig. 12. Proposed mechanism for the oxidation of *n*-octane over cobalt substituted ceria catalyst.

was also found in a mixed valence (+4/+3) state in the spent catalyst. Thus the XPS study shows a slight reduction of the catalyst. The increase in the lattice parameter of the spent Ce<sub>0.90</sub>Co<sub>0.10</sub>O<sub>2-δ</sub> catalyst compared to the freshly prepared catalyst also confirms that the catalyst is slightly reduced after four temperature cycles of oxidation of octane. However, the XRD study still shows that the compound retained its crystal structure.

### 3.2.3. Mechanistic investigations

Some investigations into the mechanism of the oxidation of *n*-octane over the Ce<sub>0.90</sub>Co<sub>0.10</sub>O<sub>2-δ</sub> catalyst have been carried out. A small amount of octane conversion occurred even in the absence of oxygen feed to the reaction. This suggested that this may likely be due to the lattice oxygen which is supplied from the catalyst. At lower temperature the catalyst follows a Mars–van Krevelen mechanism involving lattice oxide ions which generates a mixture of oxygenated alkanes by reaction of the alkanes with electrophilic oxygen species. But it is also found that the lattice oxygen is a primary oxidant to form other products such as aromatics at higher oxygen feeds and high reaction temperature. In the presence of more feed oxygen and at high temperature, the gas-phase conversion of octane over cobalt substituted ceria shows a greater selectivity toward the formation of oxygenates and aromatics, where the catalyst is in the fully oxidized state. The catalyst abstracts the hydrogen from the octane, it is consistent with the redox properties of the catalyst in which the oxide ions abstract a hydrogen from the octane and reduces the metal to lower oxidation states and continues the redox behavior of the Ce<sub>0.90</sub>Co<sub>0.10</sub>O<sub>2-δ</sub> catalyst.

A mechanism proposed for this ionic catalyst is given in Fig. 12. As seen from the proposed mechanism, the catalyst surface contains two distinct sites: (1) an electron deficient Co<sup>2+</sup> ion for adsorption of donor molecules and (2) an oxide ion site next to Co<sup>2+</sup> for the adsorption of acceptor molecules. There was no oxidation of octane on pure CeO<sub>2</sub> which clearly suggests that Ce<sup>4+</sup> and O<sup>2-</sup> sites are not active for this catalytic reaction. There are no other sites apart from the cobalt ions for the adsorption of donor and acceptor molecules in the catalyst. We have shown that in Ce<sub>1-x</sub>Co<sub>x</sub>O<sub>2-x</sub> the Co ion and the oxide ion vacancies next to each other act as redox sites and follow the dual site mechanism. Here the normal site for the adsorption of olefins is Co<sup>2+</sup> in the Ce<sub>0.90</sub>Co<sub>0.10</sub>O<sub>2-δ</sub> catalyst and the oxide ion vacancy is a nucleophilic site which is ideal for the accommodation of O<sup>2-</sup>. The formation of oxygenates, aromatics and other products will follow from the octenes formation by continuation of redox behavior of

the catalyst, because the oxidation of  $\text{Co}^{2+}$  to the  $\text{Co}^{3+}$  state induces the reduction of  $\text{Ce}^{4+}$  to the  $\text{Ce}^{3+}$  state, which is reversible.

#### 4. Conclusions

A systematic oxidation of *n*-octane has been carried out in this study. A single step solution combustion method was described to prepare a cobalt ion substituted ceria  $\text{Ce}_{0.90}\text{Co}_{0.10}\text{O}_{2-\delta}$  catalyst for the oxidation of octane. Lattice oxygen is highly activated because of the Co substitution and it plays a key role in octane oxidation and influences the oxygen storage capacity and properties such as reducibility and reduction temperature. The reactions lead to effective yields of desirable products at high selectivity under moderate conditions. Also the catalyst shows higher activity and good selectivity toward the oxygenates, octenes and  $\text{C}_8$  products like ethyl benzene, styrene and xylene.

#### Acknowledgement

We acknowledge the financial assistance from the SASOL, the University of KwaZulu-Natal (UKZN) and THRIP. The authors also thank Prof. M.S. Hegde, Indian Institute of Science (IISc), for his help and suggestions in recording the XPS data.

#### Appendix A. Supplementary data

Supplementary data associated with this article can be found, in the online version, at <http://dx.doi.org/10.1016/j.apcata.2012.09.013>.

#### References

- [1] B.C.H. Steele, *Solid State Ionics* 12 (1984) 391–406.
- [2] M. Mogensen, N.M. Sammes, G.A. Tompsett, *Solid State Ionics* 129 (2000) 63–94.
- [3] A. Tschöpe, D. Schaadt, R. Birringer, J.Y. Ying, *Nano. Mater.* 9 (1997) 423–432.
- [4] V. Perrichon, A. Laachir, G. Bergeret, R. Frety, L. Tournayan, O. Touret, *J. Chem. Soc., Faraday Trans.* 90 (1994) 773–781.
- [5] M. Ricken, J. Nölting, I. Riess, *J. Solid State Chem.* 54 (1984) 89–99.
- [6] M.A. Hasan, M.I. Zaki, L. Pasupulety, *J. Phys. Chem. B* 106 (2002) 12747–12756.
- [7] Y.-W. Zhang, R. Si, C.-S. Liao, C.-H. Yan, C.-X. Xiao, Y. Kou, *J. Phys. Chem. B* 107 (2003) 10159–10167.
- [8] K.C. Patil, *Chemistry of Nanocrystalline Oxide Materials: Combustion Synthesis, Properties and Applications*, World Scientific, 2008.
- [9] L. Vivier, D. Duprez, *ChemSusChem* 3 (2010) 654–678.
- [10] H. Wang, J.L. Ye, Y. Liu, Y.D. Li, Y.N. Qin, *Catal. Today* 129 (2007) 305–312.
- [11] S.M. de Lima, A.M. da Silva, L.O.O. da Costa, U.M. Graham, G. Jacobs, B.H. Davis, L.V. Mattos, F.B. Noronha, *J. Catal.* 268 (2009) 268–281.
- [12] J.C. Vargas, S. Libs, A.-C. Roger, A. Kiennemann, *Catal. Today* 107–108 (2005) 417–425.
- [13] H. Wang, Y. Liu, L. Wang, Y.N. Qin, *Chem. Eng. J.* 145 (2008) 25–31.
- [14] B. Zhang, X. Tang, Y. Li, Y. Xu, W. Shen, *Inter. J. Hydrogen Energy* 32 (2007) 2367–2373.
- [15] M. Benito, R. Padilla, L. Rodríguez, J.L. Sanz, L. Daza, *J. Power Source* 169 (2007) 167–176.
- [16] H. Song, L. Zhang, R.B. Watson, D. Braden, U.S. Ozkan, *Catal. Today* 129 (2007) 346–354.
- [17] G.C. Bond, D.T. Thompson, *Catal. Rev.* 41 (1999) 319–388.
- [18] P. Claus, *Appl. Catal. A* 291 (2005) 222–229.
- [19] P. Landon, P.J. Collier, A.J. Papworth, C.J. Kiely, G.J. Hutchings, *Chem. Commun.* (2002) 2058–2059.
- [20] Q. Fu, A. Weber, M. Flytzani-Stephanopoulos, *Catal. Lett.* 77 (2001) 87–95.
- [21] A.C. Gluhoi, S.D. Lin, B.E. Nieuwenhuys, *Catal. Today* 90 (2004) 175–181.
- [22] S.P. Ray, A.S. Nowick, D.E. Cox, *J. Solid State Chem.* 15 (1975) 344–351.
- [23] R.J. Farrauto, R.M. Heck, *Catal. Today* 51 (1999) 351–360.
- [24] G.R. Rao, B.G. Mishra, *Bull. Catal. Soc. 2* (2003) 122–134.
- [25] G. Ranga Rao, P. Fornasiero, R. Di Monte, J. Kašpar, G. Vlaic, G. Balducci, S. Meriani, G. Gubitosa, A. Cremona, M. Graziani, *J. Catal.* 162 (1996) 1–9.
- [26] P. Fornasiero, R. Dimonte, G.R. Rao, J. Kaspar, S. Meriani, A. Trovarelli, M. Graziani, *J. Catal.* 151 (1995) 168–177.
- [27] A. Trovarelli, C. de Leitenburg, M. Boaro, G. Dolcetti, *Catal. Today* 50 (1999) 353–367.
- [28] Y. Li, Q. Fu, M. Flytzani-Stephanopoulos, *Appl. Catal. B* 27 (2000) 179–191.
- [29] T. Baidya, G. Dutta, M.S. Hegde, U.V. Waghmare, *Dalton Trans.* (2009) 455–464.
- [30] W. Liu, M. Flytzani-Stephanopoulos, *Chem. Eng. J.* 64 (1996) 283–294.
- [31] P. Fornasiero, G.R. Rao, J. Kašpar, F. L'Erario, M. Graziani, *J. Catal.* 175 (1998) 269–279.
- [32] S. Roy, M.S. Hegde, *Catal. Commun.* 9 (2008) 811–815.
- [33] P.A. Deshpande, G. Madras, *Appl. Catal. B* 100 (2010) 481–490.
- [34] S. Sharma, P.A. Deshpande, M.S. Hegde, G. Madras, *Ind. Eng. Chem. Res.* 48 (2009) 6535–6543.
- [35] P.A. Deshpande, M.S. Hegde, G. Madras, *Appl. Catal. B* 96 (2010) 83–93.
- [36] P.A. Deshpande, M.S. Hegde, G. Madras, *AIChE J.* 56 (2010) 1315–1324.
- [37] M.S. Hegde, G. Madras, K.C. Patil, *Acc. Chem. Res.* 42 (2009) 704–712.
- [38] G.R. Rao, *Bull. Mater. Sci.* (1999) 89–94.
- [39] G.R. Rao, J. Kašpar, S. Meriani, R. Monte, M. Graziani, *Catal. Lett.* 24 (1994) 107–112.
- [40] K. Conder, E. Pomjakushina, A. Soldatov, E. Mitberg, *Mater. Res. Bull.* 40 (2005) 257–263.
- [41] L.A. Bruce, M. Hoang, A.E. Hughes, T.W. Turney, *Appl. Catal. A* 100 (1993) 51–67.
- [42] M. Kang, M.W. Song, C.H. Lee, *Appl. Catal. A* 251 (2003) 143–156.
- [43] A. Martinez-Arias, M. Fernandez-Garcia, A. Iglesias-Juez, A.B. Hungria, J.A. Anderson, J.C. Conesa, J. Soria, *Appl. Catal. B* 38 (2002) 151–158.
- [44] D. Srinivas, C.V.V. Satyanarayana, H.S. Potdar, P. Ratnasamy, *Appl. Catal. A* 246 (2003) 323–334.
- [45] M. Machida, M. Uto, D. Kurogi, T. Kijima, *J. Mater. Chem.* 11 (2001) 900–904.
- [46] J. Rodriguez-Carvajal, *F. 2k, v. 3.30, Multi-pattern Rietveld Refinement program* (June 2005).
- [47] D. Terribile, A. Trovarelli, J. Llorca, C. de Leitenburg, G. Dolcetti, *Catal. Today* 43 (1998) 79–88.
- [48] E. Garbowski, M. Guenin, M.-C. Marion, M. Primet, *Appl. Catal.* 64 (1990) 209–224.
- [49] Balkrishna B. Topea, Rabindran J. Balasamy, Alam Khurshida, Luqman A. Atanda, Hidenori Yahiro, Tetsuya Shishido, Katsuomi Takehirad, Sulaiman S. Al-Khattaf, *Appl. Catal. A* 407 (2011) 118–126.
- [50] A. Kotani, H. Ogasawara, *J. Elect. Spectro. Relat. Phenom.* 60 (1992) 257–299.
- [51] T. Blasco, J.M. Lopez Nieto, *Appl. Catal. A* 157 (1997) 117–142.
- [52] T. Blasco, J.M. Lopez Nieto, A. Dejoz, M.I. Vazquez, *J. Catal.* 157 (1995) 271–282.
- [53] E.A. Elkhalfifa, H.B. Friedrich, *Catal. Lett.* 141 (2011) 554–564.
- [54] E.A. Elkhalfifa, H.B. Friedrich, *Appl. Catal. A* 373 (2010) 122–131.
- [55] V.D.B.C. Dasireddy, S. Singh, H.B. Friedrich, *Appl. Catal. A* 421–422 (2012) 58–69.
- [56] P. Meriaudeau, A. Thangaraj, C. Naccache, S. Narayanan, *J. Catal.* 146 (1994) 579–582.
- [57] D.O. Onukwuli, H.M. Ngomo, A.A. Susu, *Petr. Sci. Tech.* 17 (1999) 711–735.
- [58] B.C. Shi, B.H. Davis, *J. Catal.* 157 (1995) 626–630.